PAPER

Poly(alkyl-biphenyl pyridinium) anion exchange membranes with a hydrophobic side chain for mono-/divalent anion separation†

Hongxin Yang,‡[a] Noor Ul Afsar,‡[a] Qian Chen,[a] Xiaolin Ge,[a] Xingya Li, [iD][a] Liang Ge*[ab] and Tongwen Xu [iD]*[a]

A series of poly(alkyl-biphenyl pyridinium) anion exchange membranes (AEMs) with a hydrophobic side chain were prepared for mono-/divalent anion separation using electrodialysis (ED). A poly(alkyl-biphenyl pyridinium) polymer was synthesized *via* superacid-catalyzed polymerization, and then quaternization was conducted using Menshutkin reactions with 1-bromopentane. The obtained quaternized product had excellent solubility in common organic solvents, making it flexible to form homogeneous membranes by a solution casting method. The introduction of a hydrophobic side chain resulted in a microphase separation structure in the membrane, which is favorable to the active transport of Cl^- (higher Cl^- flux of up to 3.37 mol m^{-2} h^{-1} at a 10 mA cm^{-2} current density) compared with that of SO_4^{2-} ions giving a high permselectivity of 11.9 in a mixed salt ($NaCl/Na_2SO_4$) system. In addition, the prepared membrane exhibited excellent alkaline stability in successive ED tests. It showed an OH^- flux of up to 3.6 mol m^{-2} h^{-1} with a permselectivity of 361.2 between OH^- and WO_4^{2-}, which is much higher than that of Neosepta ACS membrane. The ED results manifest that the poly(alkyl-biphenyl pyridinium) AEMs can be promising candidates for practical mono-/divalent anion separation in industry.

Keywords: Superacid-catalyzed polymerization; Anion exchange membrane; Mono-/divalent anion separation; Electrodialysis; Permselectivity.

1 Introduction

Electrodialysis (ED) is a membrane-based process that plays an essential role in desalination, wastewater treatment, and acid–base recovery.[1] Generally, ED concentrates and dilutes a solution with the driving force of an electrical potential difference. However, higher requirements are put forward for a particular purpose in the ED process. For example, the selective separation of monovalent anions, such as Cl^- and OH^- from divalent anions SO_4^{2-} and WO_4^{2-} using monovalent anion permselective membranes (MAPMs), is an urgent issue in the modern period for zero discharge of high salt wastewater and base recovery.[2,3] MAPMs permit the passage of monovalent anions but resist multivalent anions. The permselectivity is governed by various factors, including differences in hydrated ionic radius, Gibbs hydration free energy, and ion valence.[4] Many methods, such as introducing an oppositely charged surface layer, increasing the compactness of the membrane matrix or surface, and regulating the hydrophilicity of the membrane, have been widely investigated, and plenty of modification studies have been published elsewhere.[5–7] However, highly dense structures often lead to high area resistance, which is not conducive to the application of the ED process. The active surface layer on the membrane's surface using electrostatic interaction is weakly bound to the surface, and it can quickly disengage under harsh conditions.[8] To date, there have been no commercially available MAPMs that can work well under strongly caustic conditions. Thus, it is crucial to use a bottom-up synthetic approach to formulate a stable polymer and its transformation into a membrane for high-selectivity ion separation.

Previous studies described that electron-withdrawing groups in most AEMs based on ketone and sulfone linkages reduce the electron density of carbon (ether-connected

[a] *Anhui Provincial Engineering Laboratory of Functional Membrane Materials and Technology, Department of Applied Chemistry, School of Chemistry and Materials Science, University of Science and Technology of China, Hefei 230026, PR China. E-mail: geliang@ustc.edu.cn, twxu@ustc.edu.cn*

[b] *Applied Engineering Technology Research Center for Functional Membranes, Institute of Advanced Technology, University of Science and Technology of China, Hefei 230088, PR China.*

† Electronic supplementary information (ESI) available. See DOI: https://doi.org/10.1039/d2im00043a

‡ These authors contributed equally to this work.

carbon and benzyl carbon). As a result, this triggers aryl-ether splitting[9] (OH⁻ nucleophilic attack) and the removal of benzyl cationic quaternary ammonium (QA) head groups.[10] Introducing flexible spacers within the cationic head groups and polymer backbones may promote alkaline stability due to the hydrophilic–hydrophobic microphase separation.[11,12] As polymer backbones also greatly affect the morphology and characteristics of AEMs, numerous studies have focused on novel polymer designs.[13,14] Polymer chains with twisted structures,[15] fluorinated block polymers,[16] local densely functionalized sites on polymer backbones,[17] cross-linked polymers,[18] and superacid-catalyzed Friedel–Crafts polymerization to integrate aromatic polymers significantly raise the alkaline stability of AEMs.[19] Despite all these efforts, superacid-catalyzed step-growth polymerization of aromatic fragments has emerged as a prosperous procedure to obtain a great variety of high-performance polymers with diverse structures. This route is simplistic and metal-free, combining different aromatic or aliphatic fragments in the polymer backbone and easily consolidating side groups offering new properties.[20,21] This approach allows the development of polymers with ether-bond-free aromatic backbones, thereby extending their employment to harsh environments.[10] Various membranes comprising ether-free backbones of aromatic fragments have shown promising results for separation,[22] energy conversion, and storage.[23] However, no such research on separating monovalent ions using ED has been reported to give a realistic perspective for industrial applications. The synthesis of AEMs usually includes halomethylation of a polymer backbone followed by Menshutkin reaction to integrate desired cationic head groups. The *in situ* produced chloromethyl methyl ether is carcinogenic, which is skipped in this project to execute this method environmentally friend. Besides the backbone, an alkyltethered QA group was introduced to boost further the chemical stability, which acts as a scaffold for the cationic groups, as shown in Scheme 1.

Herein, we report a series of poly(alkyl-biphenyl pyridinium) AEMs prepared from a two-step reaction between 4-acetylpyridine and biphenyl *via* superacid-catalyzed step-growth polymerization reaction, which is free of any base-sensitive diaryl ether linkages and benzylic C–H. A co-monomer containing 4-acetylpyridine was employed to create ion transport channels by reacting with 1-bromopentane. The hydrophilic–hydrophobic phases enhance anion transport for ED application in recovery processes without sacrificing the

permselectivity. The physicochemical properties such as water uptake, swelling ratios, current–voltage curves, area resistance, and anion permeability of the poly(alkyl-biphenyl pyridinium) AEMs with different dosages of 1-bromopentane were determined and discussed in the main text. In particular, the selective separation of mono-/divalent anions in both neutral and basic systems was investigated.
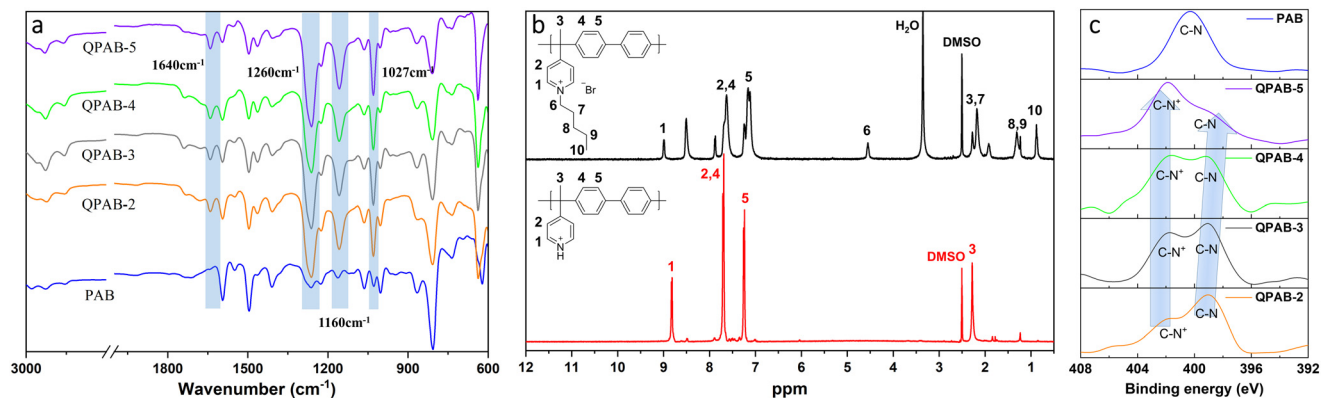
2 Results and discussion

2.1 Chemical structure analysis

The ATR-FTIR spectra of the PAB and QPAB-*x* membranes were comparatively investigated, as given in Fig. 1a. The bands observed at 3031–2974 cm⁻¹ belong to C–H stretching. In contrast, the bands at 1590 and 1490 cm⁻¹ are attributed to the aromatic C=N and C=C bonds.[13] The bands appearing at 1260, 1160, and 1027 cm⁻¹ are ascribed to the presence of triflate anions formed by pyridine and acid salt.[24] After the reaction with 1-bromopentane, a new characteristic absorption band appears at 1640 cm⁻¹, attributed to the formation of the C–N bond of the pyridinium group *via* the Menshutkin reaction.[25]

^{1}H NMR spectra also confirmed the original and quaternized polymer characterization to trace the reaction progress as shown in Fig. 1b. For understanding, all the relevant peaks are designated for structure elucidation. H1 in protonated pyridine fragments is observed at a chemical shift of 8.83 ppm due to the presence of $CF_3SO_3^-$ anions, and H2 is at 7.71 ppm. H4 and H5 on the polymer biphenyl fragments are at 7.67 and 7.24 ppm, respectively, with similar peak areas. The peak at 2.28 ppm corresponds to H3 in the methyl group. After the reaction with 1-bromopentane, the quaternized product gives an additional peak at 4.54 ppm marked as H6 in the ^{1}H NMR spectra.[26] New peaks from 0.75 to 2.38 ppm are attributed to the alkyl side chain. H1 in the newly formed pyridinium ion shifted to 9.00 ppm, and H1 in the pyridine ring without the Menshutkin reaction dropped to 8.51 ppm. The graft ratio, and even the IEC, can be accurately calculated from the relative areas of these two peaks. The overall results of ATR-FTIR and ^{1}H NMR proved the success of quaternization reaction. In addition, the difference in the series of QPAB-*x* membranes is shown in Fig. S2.† In order to obtain a clear comparison result, the PAB polymer was immersed in 1 mol L⁻¹ NaOH solution for 10 days for the deprotonation of the pyridine ring before the test, as shown in Fig. S3.†

XPS was used to characterize the chemical composition of membrane surfaces. The signal differences between the PAB and QPAB-*x* membranes are given in Fig. 1c. Due to N heteroatoms in the pyridine ring, a high resolution of XPS spectra can prove quaternization by revealing a new C–N⁺ peak next to the original C–N after the Menshutkin reaction. The peak intensity of C–N⁺ compared to that of C–N indicated the difference in quaternization degree, which grew with the increase of 1-bromopentane concentration.

Scheme 1 Synthesis route of poly(alkyl-biphenyl pyridinium) and quaternized poly(alkyl-biphenyl pyridinium).

Fig. 1 Chemical structure analysis of PAB polymer and QPAB-x membranes. (a) ATR-FTIR spectra of PAB polymer and QPAB-x membranes; (b) ^{1}H NMR spectra of PAB and the QPAB-2 membrane; (c) XPS spectra of PAB polymer and QPAB-x membranes.
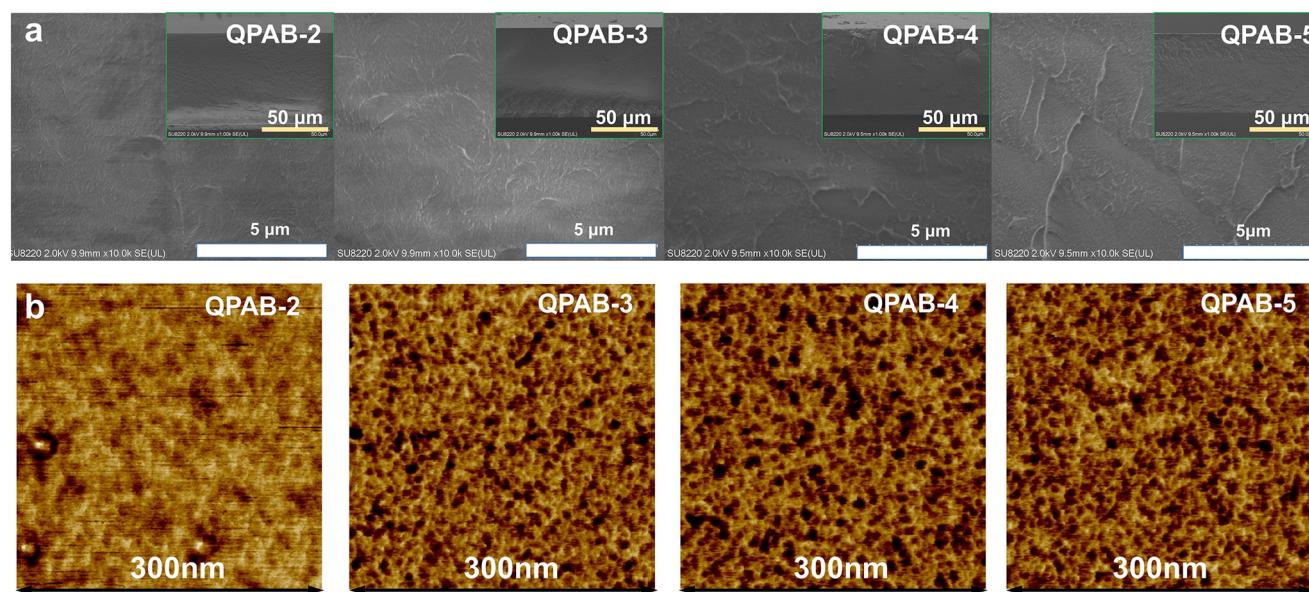
2.2 Morphology features

The SEM cross-section morphology of QPAB-x membranes shows that the homogeneous AEMs formed after quaternization, as demonstrated in Fig. 2a. And AFM images were selected to detect the phase separation morphology and ion channels to verify the spatial arrangement features of the bulk membrane,[27] as shown in Fig. 2b. The dark and bright parts of the image represent the hydrophilic and hydrophobic domains of the membrane, respectively. The hydrophilic regions penetrating through the membrane are used to form ion channels and provide electrochemical and ion transport functions; in contrast, the hydrophobic regions are used to maintain structural stability and provide mechanical properties.[28] The good morphological properties of QPAB-x membranes are displayed due to the difference in the alignment between the rigid aromatic backbone and the pyridinium cation side chain with a flexible aliphatic end. The result suggests that this series of QPAB-x membranes have an excellent microphase separation structure.

2.3 Physical and electrochemical characteristics

IEMs should have adequate water uptake to maintain smooth ion transport. However, a balanced WU is important since excessive WU may lead to undesirable membrane swelling and decrease mechanical properties, which directly affects the membrane's selectivity for hydrated multivalent ions.[29] As anticipated, the WU of AEMs increases with increasing dosage of 1-bromopentane. The WU and IEC of the synthesized QPAB-x membranes are shown in Fig. 3a as a function of 1-bromopentane dosage. It was found to be 0.9–1.4 mmol g^{-1}. The obtained IEC shows good agreement with the value obtained from the ^{1}H NMR results. The SR

Fig. 2 Morphology features of QPAB-x membranes. (a) SEM cross-section images of QPAB-x membranes; (b) AFM phase images of QPAB-x membranes.
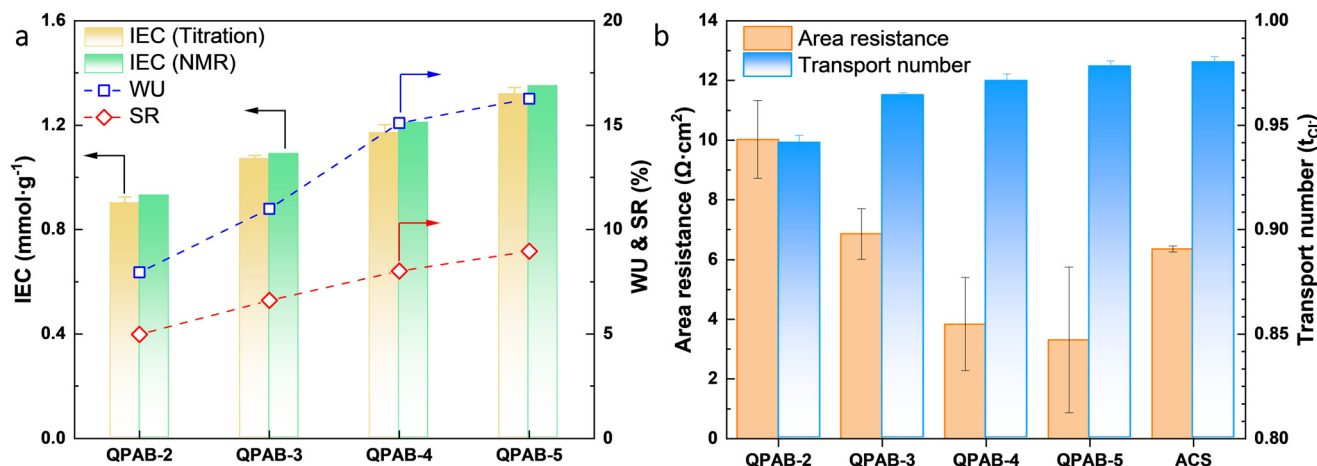
Fig. 3 Physical and electrochemical characteristics of QPAB-*x* and Neosepta ACS membranes. (a) IEC, WU and SR of QPAB-*x* membranes; (b) area resistance and transport number of QPAB-*x* and Neosepta ACS membranes.

increased with increasing IEC and was found to be 4 to 8% at 25 °C (Fig. 3a). The relatively low WU and SR proved the excellent dimensional stability of AEMs. The IEC and SR were controlled by an appropriate dosage of 1-bromopentane, which is favorable for dimensional stability.

Membrane electrochemical properties are a critical parameter in developing electrically driven membrane processes. They regulate the ion mobility energy consumption and the total cost of the ED process. Herein, the area resistances of the Neosepta ACS membrane and QPAB-*x* membranes have been found in the range of 3.3–10.0 Ω cm^2 (Fig. 3b). The area resistance decreases with increasing degree of alkyl substitution. Among them, the QPAB-2 membrane showed a high area resistance of 10.0 Ω cm^2 because of the low formation of the functional groups. Besides, the transport number was estimated by measuring the membrane potential with different concentrations of electrolyte solutions on both sides. A higher concentration of QA groups in the AEM resulted in a more pronounced effect on ion selectivity. The magnitude of the Donnan potential at the AEM-electrolyte interfaces membrane potential (E) is directly related to the transport number. The transport number of QPAB-*x* membranes was observed in the range of 0.94 to 0.98. The transport number increased with increasing IEC, exhibiting higher selectivity for anions by providing enhanced channels. This factor could contribute to decreasing of the membrane area resistance, which could be promising to improve the anion flux.

2.4 Thermal and mechanical stability

TGA showed the thermal stabilities of the PAB polymer and QPAB-*x* membranes under an N$_2$ atmosphere, and the weight loss of the membranes as a function of temperature is illustrated in Fig. 4. Remarkably, the TGA result of the base PAB polymer showed a two-step weight loss. The first step is from 30 to 100 °C, and is attributed to the evaporation of

absorbed water. And the second step belongs to backbone degradation above 450 °C with 70% residue yields. After polymer quaternization, QPAB-*x* membranes showed three stages of weight loss. The newly added stage between 200 and 410 °C is the degradation of the pyridinium-containing side chains. The thermal stability of QPAB-*x* is similar to that of the QPPO matrix, a traditional and extensively used AEM for fuel cell and ion separation.[30] This result indicates that the membranes can be applied for ion separation at high temperatures because of good thermal stability. The exceptional thermal stability could be attributed to the high aromaticity and rigidity of the copolymers. This exceptional thermal stability may offer innovative dimensions for applying ether-bond-free polymers to strengthen their thermal stability. The mechanical properties of the membranes were also tested in dry states, as shown in Table S1.† The high tensile strength and low elongation at break
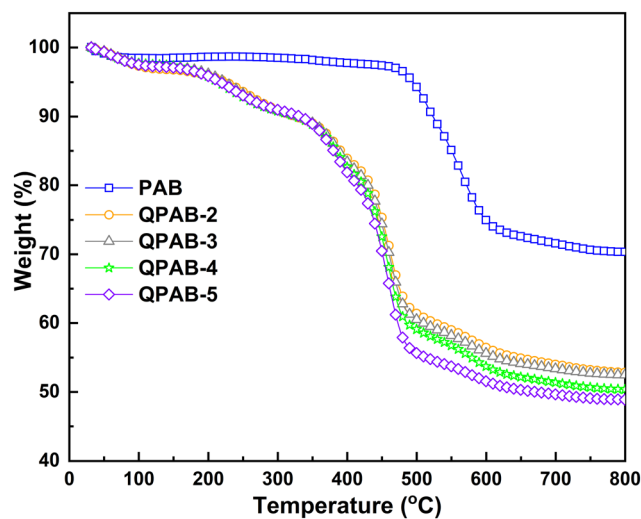

Fig. 4 TGA thermograms of PAB and QPAB-*x* membranes in a N$_2$ atmosphere.

results indicated good toughness and dimensional membrane stability, sufficient for ED applications.

2.5 Current–voltage curves

An I–V curve is used to examine the membrane resistance and limiting current density (I_{lim}), and can be employed to determine the operating current density to avoid water splitting in the ED process.[31] A lower operating current density than the I_{lim} would decrease concentration polarization. The I–V curves of the Neosepta ACS membrane and QPAB-x membranes were measured in 0.5 mol L^{-1} NaCl solution. As shown in Fig. 5a, the I–V curves of the membranes displayed a typical three-region model. The first region at low current density (ohmic region) is caused by ion transport between the solution interface and the membrane. In this region, the potential drop on the membrane is directly proportional to the applied current. In the second region, the rate of ion transport across the membrane increases, and the concentration of ions close to the interface will rapidly decrease. This region is called the plateau region, which indicates the limiting current density. The limiting current density could be calculated from dE/di vs. current density curves as given in Fig. 5b. The last region (the over limiting-current density region) is corresponding to the water splitting to produce more ions for continuous electromigration.[32]

It is worth noting that compared with those of previously reported AEMs,[33–35] the limiting current densities of QPAB-x membranes are significantly high (i.e., 110 to 155 mA cm^{-2}), and they maintain a strong positive correlation with the IEC. The high I_{lim} values of QPAB-x membranes, shown in the overall I–V curves, are due to the well-defined hydrophilic/hydrophobic micro-phase

separation enhancing the anion transport. Therefore, the low resistance, high transport number and I_{lim} values could meet various water quality and operating environment requirements, and the membranes can be used in the ED process. High limiting current density is a critical property that reflects the ability of AEMs to transport ions and indirectly determines the performance of AEMs.

2.6 Anion flux and permselectivity evaluation

The ion flux and permselectivity of the prepared membranes were evaluated for two anionic systems, i.e., 0.1 mol L^{-1} NaCl/Na$_2$SO$_4$ and 1 mol L^{-1} NaOH/0.1 mol L^{-1} Na$_2$WO$_4$. Firstly, we scanned all the membranes at 10 mA cm^{-2} to determine the best membrane based on high flux and permselectivity. Hereafter, the selected membrane was tested several times to detect its durability. The discussion can be classified into two sections for the two anionic systems.

2.6.1 Cl$^-$/SO$_4^{2-}$ system. As expected, the Cl$^-$ fluxes of QPAB-x membranes were from 3.29 to 3.37 mol m^{-2} h^{-1}, which are much higher than that of the Neosepta ACS membrane, i.e., 2.66 mol m^{-2} h^{-1} (Fig. 6a). In addition, the SO$_4^{2-}$ fluxes of QPAB-x increased with increasing IEC. These results indicated that pyridinium groups reduced the resistance of QPAB-x from 9.1 to 1.6 Ω cm^2 and increased the transport number, as discussed above. The slightly increased SO$_4^{2-}$ fluxes led to an apparent drop of permselectivity from 11.9 to 7.7. As anticipated, the increased IEC and reduced area resistance elevated the transport numbers, thus improving the flow channels for anion passage of QPAB-x membranes. The ion fluxes for all membranes increased with increasing pyridinium groups, and they obeyed the order Cl$^-$ > SO$_4^{2-}$, contrary to the order of electrostatic potentials of
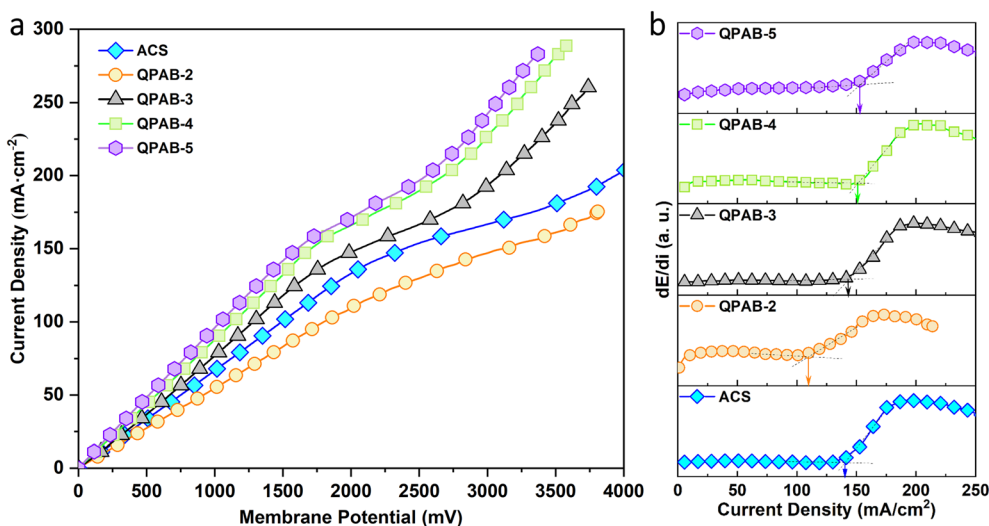

Fig. 5 (a) I–V curves of the Neosepta ACS and QPAB-x membranes; (b) the derivative dE/di as a function of current density calculated from the I–V curves.
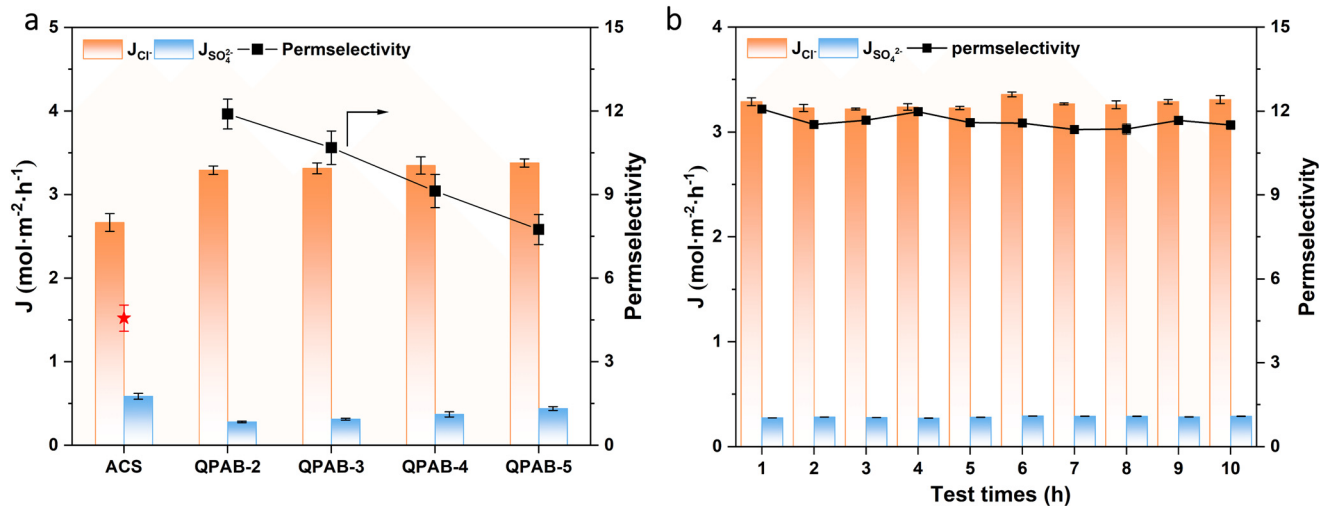
© 2023 The Author(s). Co-published by the Institute of Process Engineering, Chinese Academy of Sciences and the Royal Society of Chemistry

Ind. Chem. Mater., 2023, **1**, 129–139 | **133**

Fig. 6 (a) Anion fluxes and permselectivities of the Neosepta ACS and QPAB-*x* membranes in a NaCl/Na$_2$SO$_4$ system at a current density of 10 mA cm^{-2}; (b) cycle stability of the QPAB-2 membrane in a NaCl/Na$_2$SO$_4$ system at a current density of 10 mA cm^{-2}.

Cl$^-$ (−0.197 a.u.) and SO$_4^{2-}$ (−0.357 a.u.).[6] The dense morphology facilitated the screening out of Cl$^-$ (hydrated radius of 0.34 nm) from SO$_4^{2-}$ (0.38 nm).[36] The anion transfer properties of QPAB-*x* membranes, including anionic flux and permselectivity, are superior to those of the Neosepta ACS membrane. Taking the QPAB-2 membrane as a representative, the corresponding flux was elevated to 3.29 mol m^{-2} h^{-1}, with an increment of 23.6% compared with that of the Neosepta ACS membrane. The Neosepta ACS membrane's permselectivity was 4.6, which is two times lower than that of the QPAB-2 membrane. By comparison, the long hydrophobic alkyl chain with a cationic head carrier efficiently enhances the anion transferability of the QPAB-2 membrane. By further increasing the concentration of QA groups, the flux of the divalent anions increased, but there was nearly no change in the flux of monovalent anions, and the permselectivity decreased to 7.7, which was still higher than those of the Neosepta ACS membrane and membranes from recently published studies.[2,6] This is because increasing the QA groups to a certain limit may increase the WU of the membrane, causing swelling and providing more affinity to the hydrophilic ions (divalent ions) compared to the less hydrophilic ions (monovalent ions), thus affecting the permselectivity of membranes. For a better understanding, we compared a QPAB-*x* membrane with reported membranes. For example, comparing the QPAB-2 membrane with a mimic sandwich membrane designated as 2.5 bilayers with an IEC of 1.75 mmol g^{-1} showed a lower monovalent ion flux, and the permselectivity was not higher than 3.[2] In contrast, the QPAB-2 membrane had a lower IEC (0.90 mmol g^{-1}), but showed high flux and permselectivity (*ca.* 3 fold).

The high selectivity can be attributed to the compactness of the bulk polymer backbone and the micro-phase separation structure aided by the long alkyl spacer. The novel backbone and long alkyl spacer produced sufficient ion transport channels with low SR to control the active transport

of multivalent ions. Previously, we reported QPPO-based membranes using the Menshutkin reaction; some repulsive groups were produced and improved the permselectivity up to 7; however, the membranes showed low limiting current density and a high resistance of 25.76 Ω cm^2.[33] The dense polymer surface layer of a reported membrane greatly reduces ion flux while increasing permselectivity. This could be more obviously illustrated in the QPEI/PVA-C10-5 membrane[37] and a cross-linked amphoteric AEM.[38] Although the PAES-6C-IM membrane also contained long alkyl side-chain type AEMs,[39] our membrane is superior to it based on the final results, due to the influence of the combination of IEC, polymer backbone, the position of functional groups, *etc.* The excellent permselectivity of QPAB-*x* membranes was due to the use of a novel highly aromatic backbone that produces high micro-phase separation.

The long-term operational stability of monovalent anion-selective membranes is one of the most anticipated properties for its practicality. Here, the QPAB-2 membrane was selected as a representative for assessing the membranes' operational stability for a NaCl/Na$_2$SO$_4$ system (Fig. 6b). During 10 consecutive ED tests, there is no significant change in the Cl$^-$ flux and anion permselectivity. The operational stability of the desalination system has been confirmed.

2.6.2 OH$^-$/WO$_4^{2-}$ system. The use of AEMs for base recovery is critical to enhancing productivity; however, most AEMs based on QA groups are susceptible to highly basic species, which can degrade the polymer containing the aryl-ether linkages. Therefore, developing novel polymer-based AEMs and investigating their chemical stability under harsh conditions is crucial. The permselectivity of AEMs was increased when we changed and tuned the cationic nitrogen environment *via* introducing a new aromatic backbone without ether linkages. It benefited from changing the polarity of the QA moieties to achieve efficient base recovery
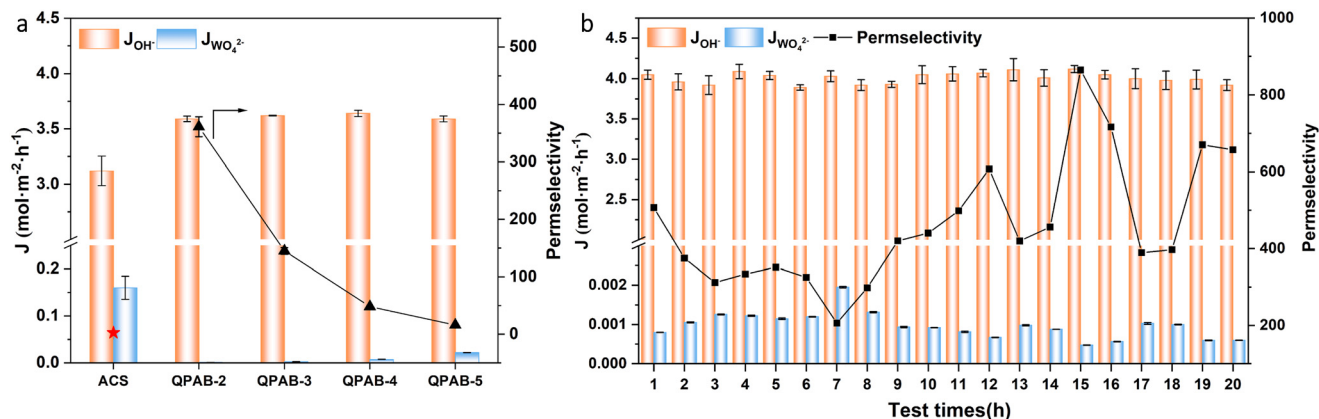
Fig. 7 (a) Anion fluxes and permselectivities of the Neosepta ACS and QPAB-x membranes in a NaOH/Na$_2$WO$_4$ system at a current density of 10 mA cm^{-2}; (b) operational stability of the QPAB-2 membrane for continuous ion selectivity.

from industrial waste, as shown in Fig. 7a. The anion flux for QPAB-x membranes improved from 3.59 to 3.64 mol m^{-2} h^{-1} by increasing the concentration of QA groups; however, the permselectivity decreased, and the lowest permselectivity was 16, observed for the QPAB-5 membrane with high multivalent ion flux, but that of the QPAB-2 membrane was as high as 361. The high selectivity could be explained based on the formation of hydrophilic–hydrophobic ion channels in the membrane caused by the hydrophilic QA and hydrophobic alkyl side chain and the main backbone. Compared with the large-sized WO$_4^{2-}$, the small OH$^-$ occupied the transfer pathways more easily and migrated through the membrane matrix more smoothly, giving rise to a higher monovalent anion permselectivity for the QPAB-2 membrane. A longer alkyl side chain grafted onto the PAB backbone resulted in a higher hydrophobicity membrane showing higher permselectivity for ions with lower hydration energy. As explained in the previous section, the increased ion channels also boosted the WU and SR for the rest of the membranes. Hence, the more hydrophilic anion WO$_4^{2-}$ makes an easy pathway that trims down permselectivity. For example, the fluxes of WO$_4^{2-}$ through the membranes increased from 0.0010 to 0.0220 mol m^{-2} h^{-1} (from QPAB-2 to QPAB-5), whereas the fluxes of monovalent anions slightly reduced. Therefore, we concluded that the dense QPAB-2 (SEM images) has a more obvious inhibitory influence on the transport of multivalent ions than on the transport of monovalent ions, resulting in a higher monovalent anion permselectivity. In contrast, the selectivity of the Neosepta ACS membrane is extremely low (2.5), which may be due to the rapid degradation of the membrane under alkaline conditions. This can be illustrated by the remarkable discoloration, as shown in Fig. S4.† After all these careful considerations, QPAB-x membranes exhibited better ion separation performances than the Neosepta ACS membrane.

The time-dependent ion flux and permselectivity of the QPAB-2 membrane are illustrated in Fig. 7b to detect operational stability for the NaOH/Na$_2$WO$_4$ system. It can be seen that the ion flux of OH$^-$ and WO$_4^{2-}$ for the membrane

in the concentrated compartment varied slightly during the whole long operation, indicating the excellent monovalent anion permselectivity performance and long-term stability under the harsh conditions for the QPAB-2 membrane. For structure confirmation, the QPAB-2 membrane after the long-time operation was characterized by ^{1}H NMR, as shown in Fig. S5.† It is important to note that aromatic pyridine-containing membranes with ether-bond-free aryl groups in the main chain possess excellent chemical stability, suggesting its implications for usage in harsh environments.

To better demonstrate the electrodialysis performance of our membrane, it was compared with other polymer AEMs, and the results show high monovalent anion flux and permselectivity at a higher current density. For instance, the QPAB-2 membrane displayed an about 16.7% higher ion flux and 140 times higher permselectivity than the Neosepta ACS membrane. Compared with the reported QPPO-C6-120 membrane (ref. 34), the outperformance the QPAB-2 membrane has been confirmed apparently.

3 Conclusions

In this work, we fabricated a series of MAPMs using a two-step route for monovalent/divalent anion separation with excellent permselectivity. With increasing degree of alkyl substitution, more anion transport channels were formed by fixing pyridinium ions to improve anion electromigration, which further leads to better electrochemical performance. Because of membrane configuration change and micro-phase separation, the IEC directly determined the membranes' permselectivity for Cl$^-$/SO$_4^{2-}$ and OH$^-$/WO$_4^{2-}$ systems. The performance of the fabricated MAPMs demonstrated that the dense ether-free polymeric backbone inhibited the transferability of large SO$_4^{2-}$ and WO$_4^{2-}$ ions while increasing the fluxes of monovalent Cl$^-$ and OH$^-$ ions so the monovalent anion permselectivity was augmented correspondingly. Reasonable long-term operational stability for commercial

© 2023 The Author(s). Co-published by the Institute of Process Engineering, Chinese Academy of Sciences and the Royal Society of Chemistry

Ind. Chem. Mater., 2023, 1, 129–139 | 135

applications was also illustrated using a single QPAB-2 membrane. In summary, this work provides a versatile approach to fabricating MAPMs with excellent permselectivity. It is promising to achieve industrial and laboratory applications in the future.

4 Experimental section

4.1 Chemicals

Biphenyl (98%), 4-acetylpyridine (98%), trifluoromethanesulfonic acid (TFSA), and trifluoroacetic acid (TFA) were obtained from Sun chemical technology (Shanghai) Co. Ltd. 1-Bromopentane was supplied by Shanghai Aladdin Biochemical Technology Co. Ltd. N-Methyl-2-pyrrolidone (NMP), anhydrous ether, dichloromethane (DCM), sodium chloride (NaCl), anhydrous sodium sulfate (Na_2SO_4), sodium hydroxide (NaOH), sodium tungstate (Na_2WO_4), and silver nitrate ($AgNO_3$) were purchased from Shanghai Sinopharm Group Chemical Reagent Co. Ltd. Deionized (DI) water was prepared using the high-pressure reverse osmosis device in our laboratory, and the conductivity was below 8 $\mu S\ cm^{-1}$.

4.2 Synthesis of polymer and membranes

The detailed synthesis strategy for the polymer and membranes is shown in Scheme 1.

(1) **Preparation of poly(alkyl-biphenyl pyridinium) (PAB).** A typical synthesis process of PAB is described as follows:[13] biphenyl (1.5421 g) was dissolved in 2.5 mL of DCM in a flask equipped with a mechanical stirrer and ice bath (~0 °C). Then, 4-acetylpyridine (1.5748 g) was added to the above solution and kept stirring for a particular time. After that, 12 mL of TFSA was slowly added to prevent a large amount of heat generation. At this time, the whole reaction system appeared as a dark-red homogeneous solution, and then 0.55 mL of TFA was added and stirred at room temperature for about 8 h. The reaction mixture was precipitated in excess water to obtain a yellow fibrous product, which was washed until the pH was neutral. The final PAB polymer was dried in a vacuum at 60 °C for 24 h and analyzed by Fourier transform infrared (FTIR) spectroscopy and hydrogen nuclear magnetic resonance (^{1}H NMR) spectroscopy.

(2) **Quaternization and preparation of membranes.** The quaternization of the PAB polymer was carried out using the following procedure: a calculated quantity of PAB polymer (2 g) was dissolved in 22 mL of NMP, and then various molar ratios of 1-bromopentane, as prescribed in Table 1, were

added into the reaction flask. The reaction mixture was stirred at 80 °C for 24 h and then collected in ethyl acetate leading to a brown-colored fiber material. Each quaternized product was designated as QPAB-x (x = 2, 3, 4, and 5) based on the different molar ratios of 1-bromopentane and PAB. For membrane preparation, 10 wt% transparent solutions of QPAB-x were prepared in NMP, cast on clean glass, and dried at 80 °C for 6 h. Then, the membranes were peeled off from the glass plate by soaking in DI water. Subsequently, QPAB-x membranes were ion-exchanged with Cl^- ions by immersing in 1.0 mol L^{-1} NaCl solution for 48 h. Before ion separation testing, the membranes were thoroughly rinsed several times and dipped in DI water to eliminate excess NaCl solution.

4.3 Membrane characterization

The prepared PAB and QPAB-x polymers were characterized using a ^{1}H NMR spectrometer (DMX 400 NMR spectrometer) using DMSO-d$_6$ as a solvent. A FTIR spectrometer (Nicolet iS10, Thermo Fisher Scientific) with an ATR (attenuated total reflection) accessory was used for functional group analysis in the range of 4000–800 cm^{-1}. Surface characteristics of QPAB-x membranes were studied by X-ray photoelectron spectroscopy (XPS) with an Al Ka X-ray source (Thermo ESCALAB250, USA). Surface and cross-sectional analyses of QPAB-x membranes were carried out by scanning electron microscopy (SEM, XT30 ESEMTMP, Holland) and atomic force microscopy (AFM, Veeco Innova SPM, UK). The thermal stability of QPAB-x membranes was investigated under an N_2 atmosphere by raising the temperature from 30 to 800 °C at a heating rate of 10 °C min^{-1} using a thermogravimetric analyzer (TGA Q5000 V3.15 Build 263).

The ion exchange capacity (IEC) of QPAB-x membranes was measured by Mohr's method. Dried membranes in Cl^- form were weighed (W_{dry}) and immersed in 0.5 mol L^{-1} Na_2SO_4 for 48 h. The freed Cl^- ions were titrated using a solution of 0.01 mol L^{-1} $AgNO_3$. The IEC (mmol g^{-1}) was calculated by using eqn (1):

$$\text{IEC} = \frac{V_{AgNO_3} - C_{AgNO_3}}{W_{dry}} \tag{1}$$

where W_{dry} (g) is the weight of the dried membrane, and V (mL) and C (mol L^{-1}) represent the volume and molar concentration of the $AgNO_3$ solution, respectively.

The water uptake (WU) and swelling ratio (SR) were measured to determine the hydrophilicity of the AEMs. Samples in Cl^- form were immersed in water at 25 °C to fully hydrate, and then the samples were taken out and surface water was removed. The wet weight and the size of the samples were measured as W_{wet} and L_{wet}, respectively. Finally, the samples were dried at 60 °C and the dry weight and size were measured as W_{dry} and L_{dry}, respectively. The WU and SR were determined by the following equations, eqn (2) and (3), respectively.

Table 1 Synthesis conditions of QPAB-x

S. No.	PAB (mmol)	1-Bromopentane (mmol)	NMP (mL)	Reaction time (h)	Temperature (°C)
QPAB-2	4.91	9.82	22	48	80
QPAB-3	4.91	14.73	22	48	80
QPAB-4	4.91	19.64	22	48	80
QPAB-5	4.91	24.55	22	48	80

$$WU\,(\%) = \frac{W_{wet} - W_{dry}}{W_{dry}} \times 100\% \qquad (2)$$

$$SR\,(\%) = \frac{L_{wet} - L_{dry}}{L_{dry}} \times 100\% \qquad (3)$$

The membranes' transport number (t_{Cl^-}) was measured using a two-compartment cell.[40] The prepared membrane was seized between two sections comprising a solution of NaCl (0.01 mol L^{-1} and 0.05 mol L^{-1}). The potential difference across the membrane was detected with a multimeter attached with two Ag–AgCl electrodes. The t_{Cl^-} was calculated using eqn (4):

$$E_m = \frac{RT}{zF}(2t_i - 1)\ln\frac{a_1}{a_2} \qquad (4)$$

where E_m (volts) is the membrane's potential, R is the universal gas constant, T is the absolute temperature (K), F is the Faraday constant, and z is the ion charge, while a_1 and a_2 are the activities of the electrolytes in the solutions, respectively.

The current–voltage (I–V) curves were measured using a four-compartment device as reported in our previous work.[41] The outer compartments were filled with a solution of 0.3 mol L^{-1} Na$_2$SO$_4$, while 0.5 mol L^{-1} NaCl was used in the two middle compartments. The current was increased gradually using a potentiostat/galvanostat (WYL1703, Hangzhou Siling Electrical Instrument Ltd.). The voltage drop across a membrane was observed with a multimeter attached with a pair of Ag–AgCl electrodes. The limiting current density value is obtained by analyzing the first derivative function of the transmembrane voltage drop (dE/di) and the applied current density. The Neosepta ACS membrane was also selected as a control membrane for comparison. The same equipment (Fig. S1†) was used for area resistance measurement using the working current density and monitoring the voltage. The area resistance (R) was calculated using eqn (5):

$$R\,(\Omega\ cm^2) = \frac{U - U_0}{I} \times S \qquad (5)$$

4.4 Anion flux and permselectivity evaluation

Monovalent anion permselectivity was measured in an ED stack containing four compartments, as shown in Fig. S1.† QPAB-x membranes were held in the center of the ED stack, whereas commercial CMX membranes were fastened on either side. The diluted compartment was filled with a 100 mL solution containing equimolar amounts (0.1 mol L^{-1}) of NaCl and Na$_2$-SO$_4$. In contrast, the concentrated compartment was filled with 100 mL of 0.01 mol L^{-1} KNO$_3$ solution. For base recovery, the diluted and concentrated compartment compositions were changed to 100 mL mixed solution (0.1 mol L^{-1} NaOH and 0.01 mol L^{-1} Na$_2$WO$_4$) and 0.01 mol L^{-1} NaOH solution, respectively. Each solution was pumped continuously *via* peristaltic pumps with a flow rate of 20 mL min^{-1} to avoid concentration

polarization. A constant current density of 10 mA cm^{-2} was used to initiate the electromigration of ions across the membrane. After 1 h of running time, the concentration of Cl$^-$ and OH$^-$ was tested by titrating with 0.01 mol L^{-1} AgNO$_3$ and 0.01 mol L^{-1} HCl, respectively. The SO$_4^{2-}$ and WO$_4^{2-}$ concentration was tested using ICP analysis (ICP-AES, Optima 7300 DV, USA). The flux of the anions (J_i) was calculated using eqn (6):

$$J_i = \frac{(C_t - C_0) \times V}{A_m \cdot t} \qquad (6)$$

where V is the volume (100 mL), C_t and C_0 represent the initial and final molar concentrations of anions in the concentrated compartment, t is the running time, and A_m is the effective area (21.00 cm^2) of the membrane. The permselectivity between Cl$^-$ and SO$_4^{2-}$ ($P_{SO_4^{2-}}^{Cl^-}$) was calculated using eqn (7). For the base recovery, the corresponding permselectivity between OH$^-$ and WO$_4^{2-}$ ($P_{WO_4^{2-}}^{OH^-}$) was calculated by a similar equation, eqn (8):

$$P_{SO_4^{2-}}^{Cl^-} = \frac{J_{Cl^-} \times C_{SO_4^{2-}}}{J_{SO_4^{2-}} \times C_{Cl^-}} \qquad (7)$$

$$P_{WO_4^{2-}}^{OH^-} = \frac{J_{OH^-} \times C_{WO_4^{2-}}}{J_{WO_4^{2-}} \times C_{OH^-}} \qquad (8)$$

where C_{Cl^-} and $C_{SO_4^{2-}}$ are the initial molar concentration of NaCl and Na$_2$SO$_4$ in the diluted compartment, respectively. C_{OH^-} and $C_{WO_4^{2-}}$ are the initial molar concentration of NaOH and Na$_2$WO$_4$ in the diluted compartment, respectively.

Author contributions

Hongxin Yang: conceptualization and methodology. Noor Ul Afsar: data curation and writing – original draft preparation. Xiaolin Ge: visualization and investigation. Xingya Li: software and writing – review and editing. Liang Ge: data curation, method validation, and writing – original draft preparation. Tongwen Xu: supervision, project administration, and acquisition.

Conflicts of interest

All authors declare that they have no conflicts of interest.

Acknowledgements

References

1 S. Al-Amshawee, M. Y. B. M. Yunus, A. A. M. Azoddein, D. G. Hassell, I. H. Dakhil and H. A. Hasan, Electrodialysis desalination for water and wastewater: A review, *J. Chem. Eng.*, 2020, **380**, 122231.

© 2023 The Author(s). Co-published by the Institute of Process Engineering, Chinese Academy of Sciences and the Royal Society of Chemistry

Ind. Chem. Mater., 2023, **1**, 129–139 | **137**

2 L. Hao, J. Liao, Y. Jiang, J. Zhu, J. Li, Y. Zhao, B. Van der Bruggen, A. Sotto and J. Shen, "Sandwich"-like structure modified anion exchange membrane with enhanced monovalent selectivity and fouling resistant, *J. Membr. Sci.*, 2018, **556**, 98–106.

3 J. Li, S. Yuan, J. Wang, J. Zhu, J. Shen and B. Van der Bruggen, Mussel-inspired modification of ion exchange membrane for monovalent separation, *J. Membr. Sci.*, 2018, **553**, 139–150.

4 L. Ge, B. Wu, D. B. Yu, A. N. Mondal, L. X. Hou, N. U. Afsar, Q. H. Li, T. T. Xu, J. B. Miao and T. W. Xu, Monovalent cation perm-selective membranes (MCPMs): New developments and perspectives, *Chin. J. Chem. Eng.*, 2017, **25**, 1606–1615.

5 A. Lejarazu-Larrañaga, Y. Zhao, S. Molina, E. García-Calvo and B. Van der Bruggen, Alternating current enhanced deposition of a monovalent selective coating for anion exchange membranes with antifouling properties, *Sep. Purif. Technol.*, 2019, **229**, 115807.

6 H. Zhang, R. Ding, Y. Zhang, B. Shi, J. Wang and J. Liu, Stably coating loose and electronegative thin layer on anion exchange membrane for efficient and selective monovalent anion transfer, *Desalination*, 2017, **410**, 55–65.

7 Y. Zhao, J. Zhu, J. Li, Z. Zhao, S. I. Charchalac Ochoa, J. Shen, C. Gao and B. Van der Bruggen, Robust Multilayer Graphene-Organic Frameworks for Selective Separation of Monovalent Anions, *ACS Appl. Mater. Interfaces*, 2018, **10**, 18426–18433.

8 M.-Q. Wang, J. Yan, H.-P. Cui and S.-G. Du, Low temperature preparation and characterization of TiO_2 nanoparticles coated glass beads by heterogeneous nucleation method, *Mater. Charact.*, 2013, **76**, 39–47.

9 S. Miyanishi and T. Yamaguchi, Analysis of the degradation mechanism of the polyarylene ether anion-exchange membrane for alkaline fuel cell and water-splitting cell applications, *New J. Chem.*, 2017, **41**, 8036–8044.

10 A. D. Mohanty, S. E. Tignor, J. A. Krause, Y.-K. Choe and C. Bae, Systematic Alkaline Stability Study of Polymer Backbones for Anion Exchange Membrane Applications, *Macromolecules*, 2016, **49**, 3361–3372.

11 Y. Zhang, W. Chen, T. Li, X. Yan, F. Zhang, X. Wang, X. Wu, B. Pang and G. He, Tuning hydrogen bond and flexibility of N-spirocyclic cationic spacer for high performance anion exchange membranes, *J. Membr. Sci.*, 2020, **613**, 118507.

12 W. Chen, Z. Fu, X. Wu, T. Li, X. Yan, X. Wang, F. Cui, S. Zhang and G. He, Micro-phase separation promoted by electrostatic field in electrospinning of alkaline polymer electrolytes: DFT and MD simulations, *Chem. Eng. Sci.*, 2022, **248**, 117171.

13 E. Cetina-Mancilla, L. I. Olvera, J. Balmaseda, M. Forster, F. A. Ruiz-Treviño, J. Cárdenas, E. Vivaldo-Lima and M. G. Zolotukhin, Well-defined, linear, wholly aromatic polymers with controlled content and position of pyridine moieties in macromolecules from one-pot, room temperature, metal-free step-polymerizations, *Polym. Chem.*, 2020, **11**, 6194–6205.

14 F. Zhang, T. Li, W. Chen, X. Wu, X. Yan, W. Xiao, Y. Zhang, X. Wang and G. He, Highly stable electron-withdrawing CO link-free backbone with branched cationic side chain as anion exchange membrane, *J. Membr. Sci.*, 2021, **624**, 119052.

15 X. Wang, C. Lin, Y. Gao and R. G. H. Lammertink, Anion exchange membranes with twisted poly(terphenylene) backbone: Effect of the N-cyclic cations, *J. Membr. Sci.*, 2021, **635**, 119525.

16 J. E. Chae, S. Y. Lee, S. Y. Baek, K. H. Song, C. H. Park, H.-J. Kim and K.-S. Lee, High-performance multiblock PEMs containing a highly acidic fluorinated-hydrophilic domain for water electrolysis, *J. Membr. Sci.*, 2021, **638**, 119694.

17 F. Zhang, T. Li, W. Chen, X. Wu, X. Yan, W. Xiao, Y. Zhang, X. Wang and G. He, Electron-Donating $C-NH_2$ Link Backbone for Highly Alkaline and Mechanical Stable Anion Exchange Membranes, *ACS Appl. Mater. Interfaces*, 2021, **13**, 10490–10499.

18 G. Singh, M. Kumar, T. S. Thomas, T. C. Nagaiah and D. Mandal, Pendent Persubstituted Imidazolium and a Polyimidazolium Cross-Linked Polymer as Robust Alkaline Anion Exchange Membranes for Solid-State Zn–Air Batteries, *ACS Appl. Energy Mater.*, 2021, **12**, 14689–14699.

19 J. S. Olsson, T. H. Pham and P. Jannasch, Poly(arylene piperidinium) Hydroxide Ion Exchange Membranes: Synthesis, Alkaline Stability, and Conductivity, *Adv. Funct. Mater.*, 2018, **28**, 1702758.

20 Z. Li, R. Yu, C. Liu, J. Zheng, J. Guo, T. A. Sherazi, S. Li and S. Zhang, Preparation and characterization of side-chain poly(aryl ether ketone) anion exchange membranes by superacid-catalyzed reaction, *Polymer*, 2021, **222**, 123639.

21 X. Du, H. Zhang, Y. Yuan and Z. Wang, Constructing micro-phase separation structure to improve the performance of anion-exchange membrane based on poly(aryl piperidinium) cross-linked membranes, *J. Power Sources*, 2021, **487**, 229429.

22 X. Du, Z. Wang, H. Zhang, Y. Yuan, H. Wang and Z. Zhang, Prepared poly (aryl piperidinium) anion exchange membranes for acid recovery to improve dialysis coefficients and selectivity, *J. Membr. Sci.*, 2021, **619**, 118805.

23 N. Chen, H. H. Wang, S. P. Kim, H. M. Kim, W. H. Lee, C. Hu, J. Y. Bae, E. S. Sim, Y.-C. Chung and J.-H. Jang, Poly (fluorenyl aryl piperidinium) membranes and ionomers for anion exchange membrane fuel cells, *Nat. Commun.*, 2021, **12**, 2367.

24 E. M. Maya, E. Verde-Sesto, D. Mantione, M. Iglesias and D. Mecerreyes, New poly(ionic liquid)s based on poly(azomethine-pyridinium) salts and its use as heterogeneous catalysts for CO_2 conversion, *Eur. Polym. J.*, 2019, **110**, 107–113.

25 Z. Yang, M. Zhang, Z. Zhao, W. Lan, X. Zhang and M. Fan, Highly alkaline stable fully-interpenetrating network poly (styrene-co-4-vinyl pyridine)/polyquaternium-10 anion exchange membrane without aryl ether linkages, *Int. J. Hydrogen Energy*, 2022, **47**, 16580–16596.

26 L. Wang, Y. Liu and J. Wang, Crosslinked anion exchange membrane with improved membrane stability and conductivity for alkaline fuel cells, *J. Appl. Polym. Sci.*, 2019, **136**, 48169.

27 C. G. Arges and M. Dolejsi, Interconnected ionic domains enhance conductivity in microphase separated block copolymer electrolytes, *J. Mater. Chem. A*, 2017, **5**, 5619–5629.

28 Z. Yuan, L. Din, L. Xian, M. A. Shehzad and T. W. Xu, Beneficial use of rotatable-spacer side-chains in alkaline anion exchange membranes for fuel cells, *Energy Environ. Sci.*, 2018, **11**, 3472–3479.

29 Ö. Tekinalp, P. Zimmermann, O. S. Burheim and L. Deng, Designing monovalent selective anion exchange membranes for the simultaneous separation of chloride and fluoride from sulfate in an equimolar ternary mixture, *J. Membr. Sci.*, 2023, **666**, 121148.

30 V. Vijayakumar, T. Y. Son, H. J. Kim and S. Y. Nam, A facile approach to fabricate poly(2,6-dimethyl-1,4-phenylene oxide) based anion exchange membranes with extended alkaline stability and ion conductivity for fuel cell applications, *J. Membr. Sci.*, 2019, **591**, 117314.

31 N. White, M. Misovich, A. Yaroshchuk and M. L. Bruening, Coating of Nafion Membranes with Polyelectrolyte Multilayers to Achieve High Monovalent/Divalent Cation Electrodialysis Selectivities, *ACS Appl. Mater. Interfaces*, 2015, **7**, 6620–6628.

32 T. Belloň, P. Polezhaev, L. Vobecká, M. Svoboda and Z. Slouka, Experimental observation of phenomena developing on ion-exchange systems during current-voltage curve measurement, *J. Membr. Sci.*, 2019, **572**, 607–618.

33 X. Xiao, M. A. Shehzad, A. Yasmin, Z. Ge, X. Liang, F. Sheng, W. Ji, X. Ge, L. Wu and T. W. Xu, Anion permselective membranes with chemically-bound carboxylic polymer layer for fast anion separation, *J. Membr. Sci.*, 2020, **614**, 118553.

34 C. Li, G. Wang, D. Yu, F. Sheng, M. A. Shehzad, T. He, T. Xu, X. Ren, M. Cao, B. Wu and L. Ge, Cross-linked anion exchange membranes with hydrophobic side-chains for anion separation, *J. Membr. Sci.*, 2019, **581**, 150–157.

35 N. U. Afsar, X. Li, Y. Zhu, Z. Ge, Y. Zhou, Z. Zhao, A. Hussain, L. Ge, R. Fu, Z. Liu and T. W. Xu, In-situ interfacial polymerization endows surface enrichment of COOH groups on anion exchange membranes for efficient Cl^-/SO_4^{2-} separation, *J. Polym. Sci.*, 2022, **60**, 3022–3034.

36 Y. Marcus, Ionic radii in aqueous solutions, *Chem. Rev.*, 1988, **88**, 1475–1498.

37 M. Li, W. Li, X. Zhang, C. Wu, X. Han and Y. Chen, Polyvinyl alcohol-based monovalent anion selective membranes with excellent permselectivity in selectrodialysis, *J. Membr. Sci.*, 2021, **620**, 118889.

38 J. Liao, X. Yu, N. Pan, J. Li, J. Shen and C. Gao, Amphoteric ion-exchange membranes with superior mono-/bi-valent anion separation performance for electrodialysis applications, *J. Membr. Sci.*, 2019, **577**, 153–164.

39 J. Liao, X. Yu, Q. Chen, X. Gao, H. Ruan, J. Shen and C. Gao, Monovalent anion selective anion-exchange membranes with imidazolium salt-terminated side-chains: Investigating the effect of hydrophobic alkyl spacer length, *J. Membr. Sci.*, 2020, **599**, 117818.

40 J. Li, M. L. Zhou, J. Y. Lin, W. Y. Ye, Y. Q. Xu, J. N. Shen, C. J. Gao and B. Van der Bruggen, Mono-valent cation selective membranes for electrodialysis by introducing polyquaternium-7 in a commercial cation exchange membrane, *J. Membr. Sci.*, 2015, **486**, 89–96.

41 N. U. Afsar, M. A. Shehzad, M. Irfan, K. Emmanuel, F. Sheng, T. T. Xu, X. Ren, L. Ge and T. W. Xu, Cation exchange membrane integrated with cationic and anionic layers for selective ion separation via electrodialysis, *Desalination*, 2019, **458**, 25–33.

© 2023 The Author(s). Co-published by the Institute of Process Engineering, Chinese Academy of Sciences and the Royal Society of Chemistry

Ind. Chem. Mater., 2023, **1**, 129–139 | **139**